Preprint Title Synthesis of P- and N-doped carbon catalysts for the oxygen reduction reaction via controlled phosphoric acid treatment of folic acid

Authors Rieko Kobayashi, Takafumi Ishii, Yasuo Imashiro and Jun-ichi Ozaki

Article Type Full Research Paper

ORCID® iDs Jun-ichi Ozaki - https://orcid.org/0000-0002-1369-9004

Synthesis of P- and N-doped carbon catalysts for the oxygen reduction reaction via controlled phosphoric acid treatment of folic acid

Rieko Kobayashi[1], Takafumi Ishii[1], Yasuo Imashiro[1,2], and Jun-ichi Ozaki[*1]

[1]Graduate School of Science and Technology, Gunma University, 1-5-1 Tenjin-cho, Kiryu, Gunma 376-8515, Japan

[2]R&D Center, Nissinbo Holdings Inc., 1-2-3 Onodai, Midori-ku, Chiba 267-0056, Japan

Email: Jun-ichi Ozaki - jozaki@gunma-u.ac.jp

*Corresponding author.

Abstract

Herein, we synthesized N- and P-doped carbons (PN-doped carbons) by controlled phosphoric acid treatment (CPAT) of folic acid (FA) and probed their ability to catalyze the oxygen reduction reaction at the cathode of a fuel cell. Precursors obtained by heating FA in the presence of phosphoric acid at temperatures of 400–1000 °C were further annealed at 1000 °C to afford PN-doped carbons. The extent of precursor P-doping was maximized at 700 °C, and the use of higher temperatures resulted in activation and increased porosity rather than in increased P content. The P/C atomic ratios of PN-doped carbons were well correlated with those of precursors, which indicated that CPAT was

well suited for the preparation of PN-doped carbons. Carbon prepared using a CPAT temperature of 700 °C exhibited the highest oxygen reduction reaction (ORR) activity and was shown to contain –C–PO_2 and –C–PO_3 moieties as the major P species and pyridinic N as the major N species; moreover, no N–P bonds were detected. The presence of –C–PO_2 and –C–PO_3 units was concluded to decrease the work function and thus raise the Fermi level above the standard O_2/H_2O reduction potential, which resulted in enhanced ORR activity. Finally, CPAT was concluded to be applicable to the synthesis of PN-doped carbons from N-containing organic compounds other than FA.

Keywords

folic acid; oxygen reduction reaction; phosphoric acid treatment; PN-doped carbon catalysts; polymer electrolyte fuel cells

Introduction

The widespread application of fuel cells as clean energy sources is the most desirable way of realizing a low-CO_2-emission society. In conventional polymer electrolyte fuel cells (PEFCs), both anode and cathode reactions are catalyzed by Pt. Compared to the anode reaction, the cathode reaction, namely the oxygen reduction reaction (ORR), is rather slow and hence requires the use of larger amounts of Pt,[1] which increases the cost of PEFCs and prevents their wide application as domestic, back-up, and vehicle power sources. The cost of cathode catalysts can be reduced in a number of ways, e.g., by alloying Pt with

base metals,[2] forming core-shell particles with base-metal cores covered by thin Pt layers,[3] and developing non-Pt catalysts. In particular, the implementation of non-Pt or non-precious-metal cathode catalysts is the ultimate goal of PEFC development.

Since the discovery of the ORR activity of cobalt phthalocyanine in 1964,[4] numerous studies have focused on the synthesis of non-precious metal ORR catalysts such as those based on carbon,[5] e.g., thermal treatment of carbon materials impregnated with N_4-M complexes was found to afford highly active and durable ORR catalysts. Since then, much effort has been directed at clarifying the nature of the active sites in these catalysts; for example, ORR activity has been predominantly ascribed to N_x-M (M = Co, Fe) moieties on the surface of carbon supports.[6-7] Our research group has identified and characterized different types of non-Pt ORR catalysts, the so-called carbon alloy catalysts (CACs).[8] Originally, we prepared two types of CACs (nanoshell-containing carbons[9-10] and BN-doped carbons[11]) and further improved their ORR activity and durability to afford a commercial CAC[12-13] and thus realized the world's first portable PEFC cell containing a non-precious-metal cathode catalyst.[14-15]

Much effort has been directed at the development of transition-metal-free carbon catalysts for the ORR, with the best practical performance so far observed for N-doped carbons.[16] For example, a recently reported metal-free catalyst based on N-doped carbon nanotubes showed high ORR activity even under acidic conditions and allowed for facile electricity generation when employed as a single-cell cathode.[17] The ORR activity of carbon-based catalysts can be

substantially improved by their simultaneous doping with N and other elements. In 2007, we reported that carbon prepared by carbonization of a N- and B-doped furan resin exhibited an increased ORR activity in sulfuric acid solution,[11] and since then, much attention has been directed at the activation of carbon catalysts by the co-doping technique.[18] The concept of co-doping has been even extended to three-component catalysts, as exemplified by studies on N, P, S-doped and N, P, F-doped carbons.[19-20] Strelko et al. used theoretical methods to establish an interesting relationship between the band gap energy of a given catalyst and its ability to promote reactions involving electron transfer.[21] Moreover, P-doping of graphitic layers was revealed to have an effect similar to that of N-doping and hence, co-doping with P and N was found to be an effective way of increasing the ORR activity of carbons.[22-26] Most of the reported PN-doping techniques involve the carbonization of [N-containing polymer + P-containing compound] mixtures or of ionic liquids containing both N and P, i.e., employ special compounds or their combinations as starting materials.

Herein, to establish a more generalized PN-doping method allowing the use of more common compounds, we developed the technique of controlled phosphoric acid treatment (CPAT) that is potentially applicable to non-special N-containing organic compounds and applied it to folic acid (FA) as a commonly occurring N-containing organic compound. During CPAT, phosphoric acid (PA) acts as both a P-doping agent[27-28] and a chemical activator to introduce pores.[29-30] In the present study, PN-doped precursors synthesized at CPAT temperatures of 400–800 °C were carbonized at 1000 °C to prepare PN-doped

carbons, and factors influencing the ORR catalytic activity of these carbons were investigated in detail.

Results

Elemental composition and chemical structure of precursors

CPAT temperature affected both the BET specific surface area (BET-SSA) and surface elemental composition of precursors, as exemplified by values derived from X-ray photoelectron spectra of P-series precursors (Table 1). The BET-SSAs of samples prepared at CPAT temperatures of ≤700 °C were estimated as several $m^2\ g^{-1}$ but rapidly increased at temperatures above 800 °C, with maximum values obtained at 1000 °C. This behavior was different from that of H-series precursors.

Table 1: Surface properties of H- and P-type precursors.

Sample	BET-SSA ($m^2\ g^{-1}$)	Surface composition (at%)			
		C	N	O	P
H-400	20	61.7	12.7	25.6	–
H-500	65	67.2	16.3	16.5	–
H-600	115	61.4	13.1	25.5	–
H-700	56	79.2	7.2	13.6	–
H-1000	84	81.5	4.5	14.0	–
P-400	2	76.0	3.5	19.6	0.8
P-500	7	72.6	4.3	21.2	1.9

P-600	8	70.2	6.2	20.1	3.6
P-700	6	50.0	7.2	35.1	7.7
P-800	277	68.2	6.5	20.2	5.1
P-1000	1014	84.0	3.6	10.5	1.8

The results of X-ray photoelectron spectroscopy (XPS) analysis demonstrated that when pretreatment was performed in the absence of PA, the N content of carbons decreased with increasing temperature. On the other hand, in the presence of PA, the N/C atomic ratio initially increased with increasing CPAT temperature, reached a maximum at 700 °C, and then decreased. The O/C ratio behaved similarly to the N/C ratio irrespective of the presence of PA but could not be accurately estimated because of the effects of atmospheric moisture and oxygen. The P/C ratio of P-series precursors was maximal at a CPAT temperature of 700 °C, i.e., behaved similarly to the N/C ratio. Thus, CPAT promoted both the development of specific surface area and P doping, and the relative contributions of these roles were determined by temperature, i.e., P-doping was dominant below 700 °C, while chemical activation was dominant at higher temperatures. Figure 1 shows the correlation between P/C and N/C ratios in P-series precursors and HP-series carbons.

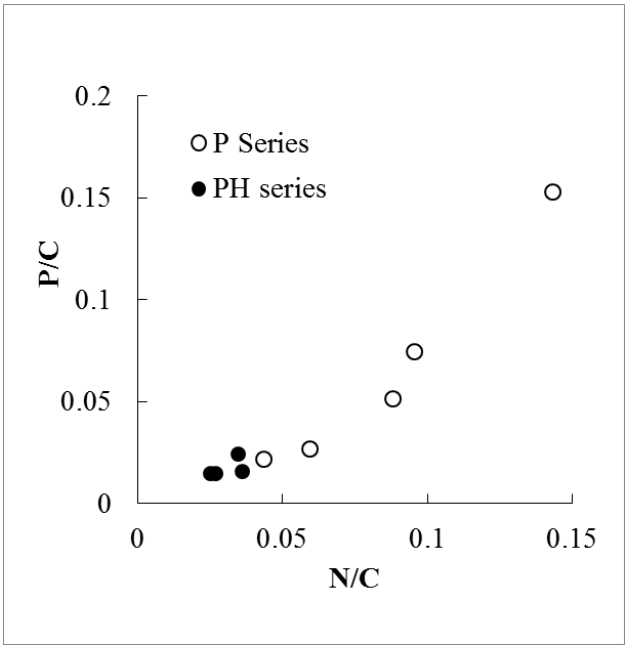

Figure 1: Correlations between P/C and N/C atomic ratios of P-series precursors (open circles) and HP-series carbons (closed circles).

The chemical states of N in P-series precursors were studied by XPS (Figs. 2(a) and (b)), which revealed that the shapes of N 1s spectra depended on pretreatment temperature and the presence/absence of PA. H-series precursors featured N 1s spectra with two peaks, the positions of which were affected by CPAT temperature (Fig. 2(a)). For FA pretreated at 500 °C (H-500), these peaks were located at 398.5 and 400.0 eV, while for H-700, peaks at 397.9 and 400.5 eV were observed, and for H-1000, signals were detected at 398.5 and 401.1 eV. The broad N 1s spectra (Fig. 2(b)) of P-series precursors prepared at 500 and 700 °C were assumed to be a superposition of several peaks. For example, the spectrum of P-500 was deconvoluted into peaks at 398.5, 400.5, and 402.5 eV, while that of P-700 was deconvoluted into peaks at 398.5, 399.8, and 401.0 eV. In contrast, the N 1s spectrum of P-1000 featured two overlapping peaks centered at 398.5 and 401.7 eV.

Conventionally, peaks at 398.5, 400.5, 401, and 402 eV in the N 1s spectra of N-doped carbons are assigned to pyridinic, pyrrole/pyridone-type, quaternary, and oxygen-bonded (oxidized) N, respectively. Thus, P-500 contained oxidized N, whereas H-500 and P-700 did not. However, P-700 contained quaternary N incorporated into graphite layers, as exemplified by the corresponding peaks at 401–400.7 eV. The peak of pyridinic N (398.5 eV), clearly observed for H-series precursors, was less pronounced in the case of P-series precursors, e.g., the intensity of this peak was higher for H-1000 than for P-1000.

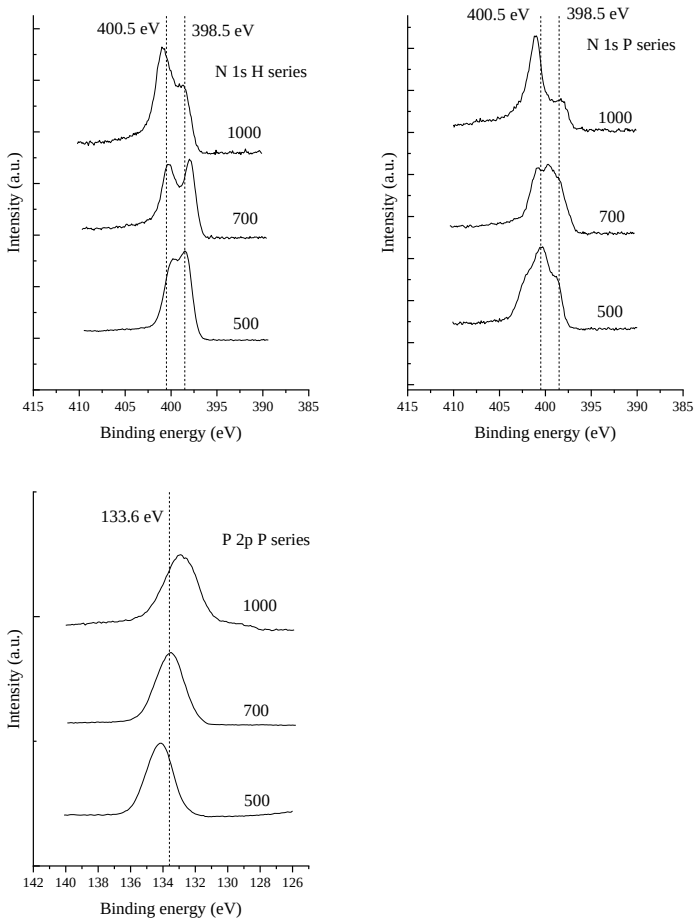

Figure 2: N 1s spectra of (a) H-series and (b) P-series precursors. (c) P 2p spectra of P-series precursors.

Structure, chemical composition, and electronic properties of carbonized FA

PH-series carbons were prepared by thoroughly rinsing P-series precursors with water to remove excess PA and subjecting them to carbonization at 1000 °C. The same operation was also performed for H-series precursors to afford HH-series carbons. The BET-SSAs of these two carbon series exhibited different behaviors (Table 2), e.g., those of HH-series carbons were almost constant (~30 $m^2\ g^{-1}$) even though the corresponding precursors showed variable BET-SSAs, whereas the BET-SSA of PH-series carbons increased with increasing CPAT temperature. Specifically, PH-700 and PH-800 had remarkably high SSAs of 674 and 730 $m^2\ g^{-1}$, respectively.

Table 2: BET-SSAs and XPS-determined elemental surface compositions of HH- and PH-series carbons.

Sample	BET SSA ($m^2\ g^{-1}$)	Surface composition (at%)			
		C	N	O	P
HH-400	34	83.7	4.6	11.8	-
HH-500	32	81.6	3.5	14.9	-
HH-600	30	81.2	2.7	16.2	-
HH-700	32	81.3	3.5	15.2	-
H-1000	84	81.5	4.5	14.0	-
PH-400	48	83.0	2.2	13.6	1.23
PH-500	243	82.3	3.0	13.5	1.3

PH-600	311	82.4	2.1	14.3	1.2
PH-700	674	81.6	2.8	13.6	1.98
PH-800	730	80.4	3.5	14.5	1.59
P-1000	1014	84.0	3.6	10.5	1.82

Table 2 also lists N/C and P/C atomic ratios determined by XPS, demonstrating that for HH- and PH-series carbons, the former ratio showed no clear dependence on pretreatment temperature and was in the range of 0.03–0.05. Conversely, the P/C atomic ratio of PH-series carbons varied in the range of 0.015–0.024, with a maximum value obtained at 700 °C. Figure 3 shows the relationship between the elemental composition of precursors and that of carbons, revealing that the N content of precursors had no influence on that of carbons, while the P content of PH-series carbons was positively correlated with that of P-series precursors. These results confirmed the viability of the CPAT method and demonstrated that carbons with a high extent of P-doping can be prepared from precursors with a high P/C atomic ratio.

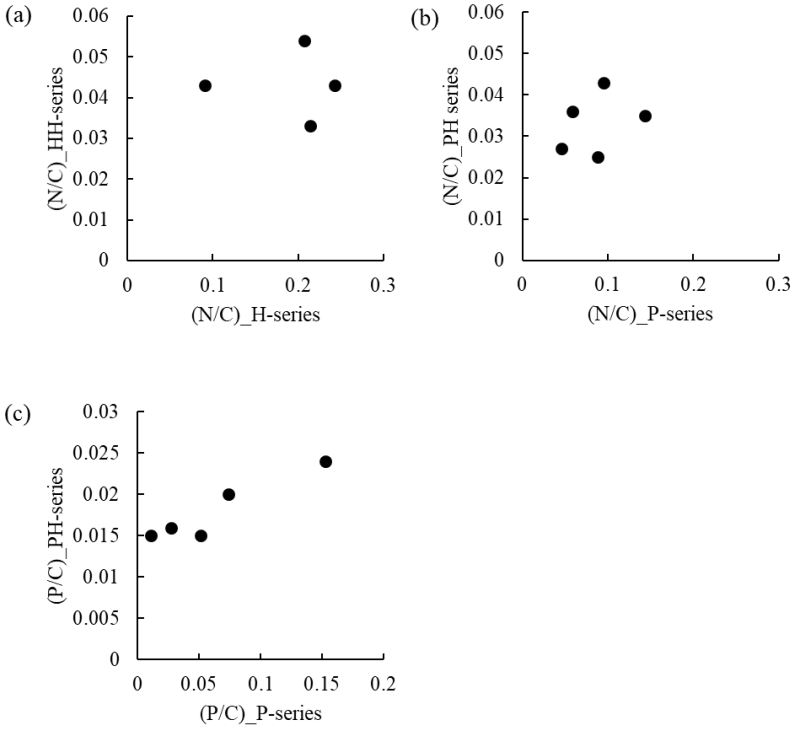

Figure 3: Correlations between (a) N/C ratios of HH-series carbons and those of H-series precursors, (b) N/C ratios of PH-series carbons and those of P-series precursors, (c) P/C ratios of PH-series carbons and those of P-series precursors.

Figures 4(a) and (b) show that although the N 1s spectra of both HH- and PH-series carbons comprised two peaks, the relative intensities of these two peaks were different, as exemplified by the spectra of H-1000 and P-1000. The shapes of the N 1s spectra of other HH- and PH-series carbons were similar to those of H-1000 and P-1000 spectra, respectively, and did not depend on pretreatment temperature. The N 1s spectra were deconvoluted into the four abovementioned peaks (pyridinic, pyrrole/pyridone-type, quaternary, and oxidized N), with the results presented in Table 3. Notably, the spectra of PH-series carbons were dominated by peaks of non-pyridinic N, while those of HH-series carbons featured signals of pyridinic and pyrrole/pyridone-type N of comparable intensities.

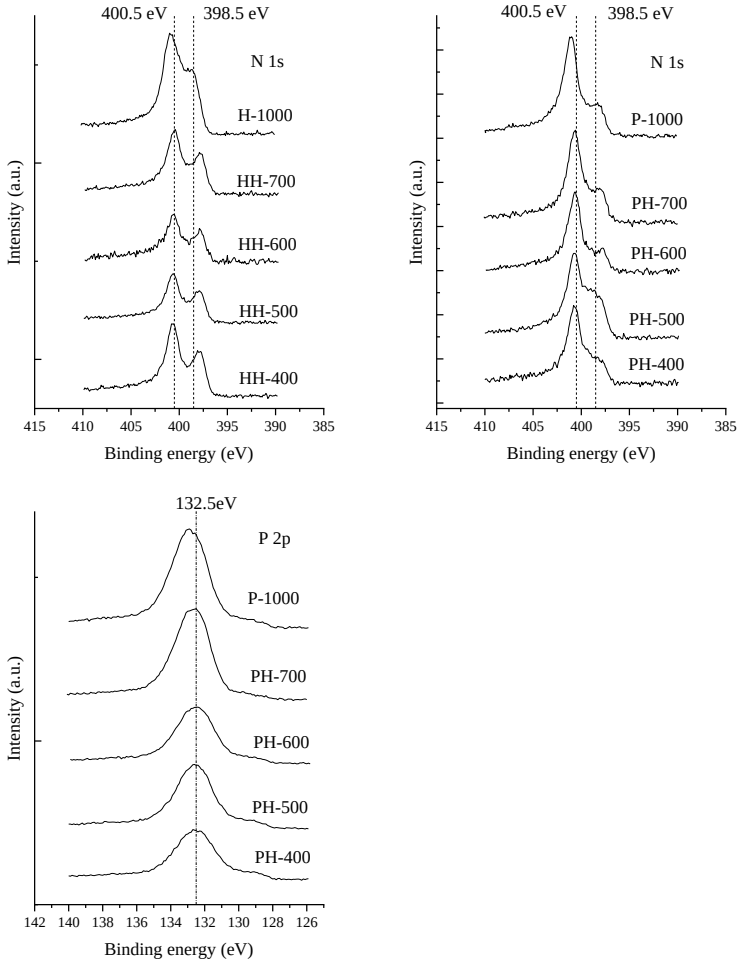

Figure 4: N 1s spectra of (a) HH- and (b) PH-series carbons. (c) P 2p spectra of PH-series carbons.

Table 3: Distribution of N-species in HH- and PH-series carbons.

Sample	N/C	$N_{pyridine}$	N_{pyrrol}	$N_{quaternary}$	N_{oxide}
HH-400	0.054	0.37	0.63	0.00	0.01
HH-500	0.043	0.32	0.44	0.00	0.23
HH-600	0.033	0.34	0.48	0.00	0.17
HH-700	0.043	0.32	0.47	0.00	0.21

H-1000	0.055	0.31	0.45	0.00	0.24
PH-400	0.027	0.23	0.60	0.00	0.17
PH-500	0.036	0.31	0.52	0.00	0.17
PH-600	0.025	0.20	0.62	0.00	0.18
PH-700	0.035	0.24	0.61	0.00	0.15
PH-800	0.043	0.31	0.45	0.00	0.24
P-1000	0.043	0.20	0.47	0.00	0.33

The P 2p spectra of all PH-series carbons featured broad asymmetric signals at 132.5 eV (Fig. 4(c)) that were deconvoluted into five components (Table 4). The most abundant and second most abundant moieties were identified as –C–PO_2 (P2) and –C–PO_3 (P3), respectively, and the contributions of other components (P1 (C–P): P bonded only to carbon atoms, P4 (–C-O–PO_3: P bonded to carbon via oxygen, P5 (P_2O_5): P without any bonds to carbon) were found to be minor.[31]

Table 4: Distribution of P-species in PH-series carbons.

Sample	P/C	P1 (P) (130 eV)	P2 (–C–PO_2) (132.5 eV)	P3 (–C–PO_3) (133.2 eV)	P4 (–C–O–PO_3) (134.2 eV)	P5 (P_2O_5) (135.6 eV)
PH-400	0.015	0.13	0.50	0.16	0.16	0.04
PH-500	0.016	0.10	0.52	0.19	0.15	0.04
PH-600	0.015	0.10	0.59	0.18	0.09	0.04
PH-700	0.024	0.04	0.46	0.31	0.16	0.04

PH-800	0.020	0.04	0.47	0.32	0.08	0.08
P-1000	0.022	0.05	0.45	0.39	0.06	0.04

The above observations revealed that carbonization at 1000 °C attenuated the differences in the chemical states of P and N observed for precursors; however, the effects of CPAT such as changes in the chemical states of N and the amount of P were retained.

The work function of PH-series carbons was determined by the vibration capacitance (Kelvin) method and fluctuated in the range of 5.4–5.6 eV (Fig. 5), decreasing with increasing CPAT temperature in the range of 400–700 °C and increasing with increasing CPAT temperature above 700 °C. As a result, the smallest work function was observed for PH-700.

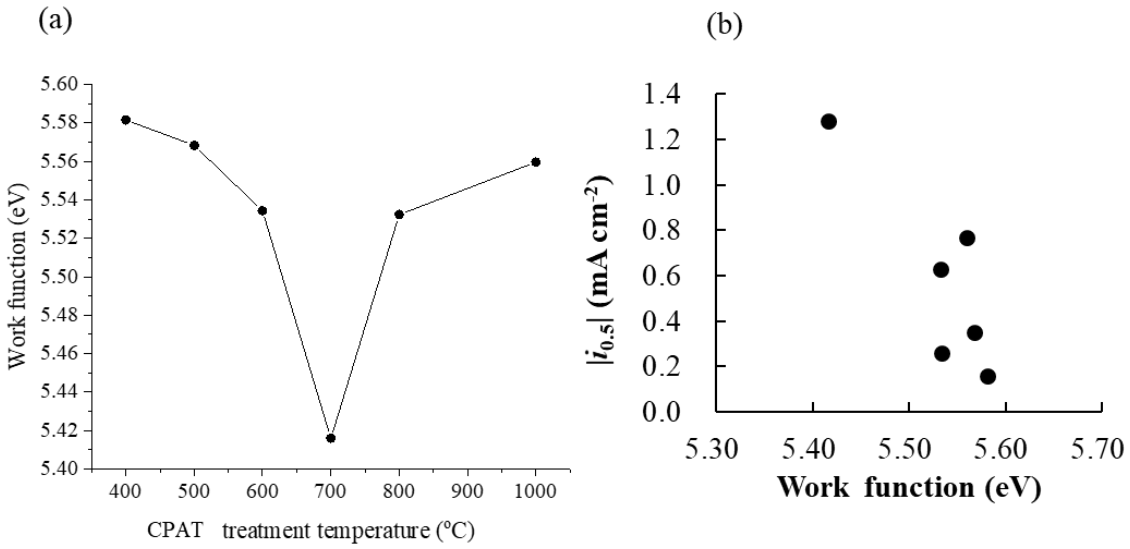

Figure 5: (a) Effect of CPAT temperature on the work function of PH-series carbons, (b) relationship between the ORR activity and work function of carbonized samples.

ORR activity of carbons

Figure 6(a) shows representative ORR voltammograms of PH- and HH-series carbons recorded in O_2-saturated aqueous H_2SO_4. The voltammograms of HH-500 and HH-700 were almost identical, i.e., pretreatment had no effect on ORR activity, while the voltammogram of H-1000 was different, showing a larger increase of ORR current density below 0.4 V vs. RHE. At a given potential, higher current densities were observed for PH-series carbons than for HH-series ones, which was ascribed to the influence of CPAT.

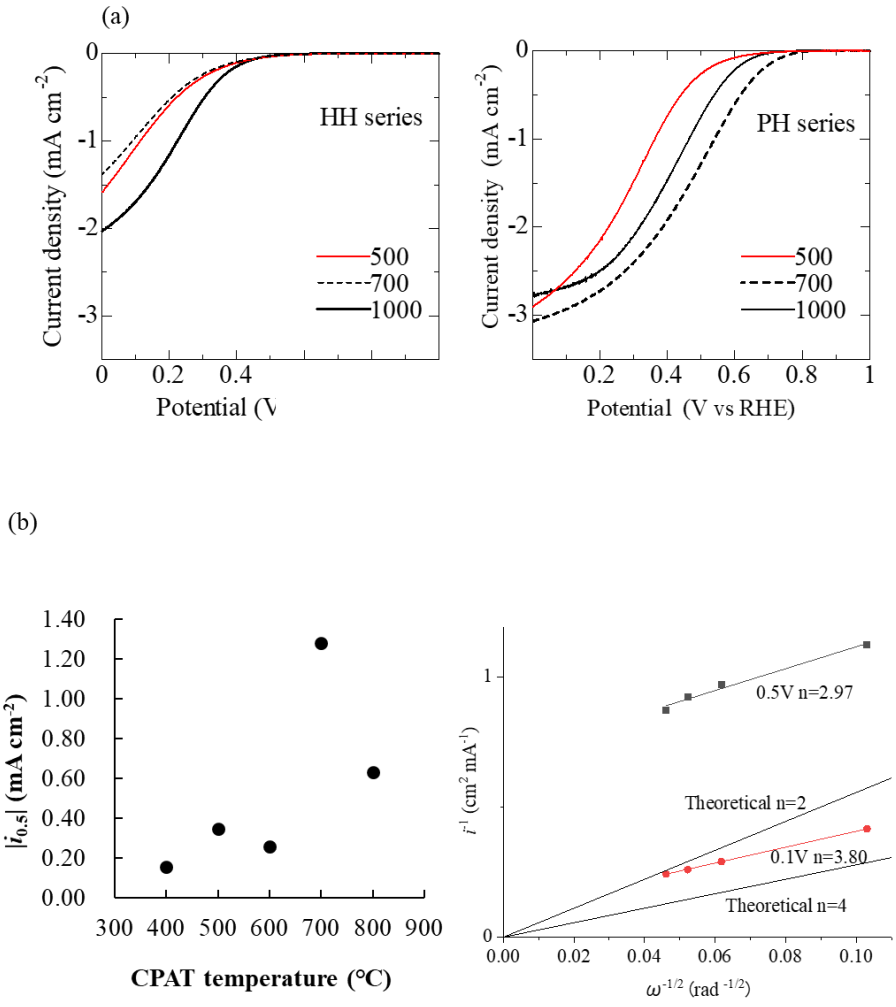

Figure 6: Results of ORR activity studies. (a) ORR voltammograms of HH- and

PH-series carbons recorded in 0.5 M O_2-saturated aqueous H_2SO_4. (b) Dependence of ORR activity (represented by E_{O2} or $i_{0.5}$) on CPAT temperature. (c) Koutecky-Levich plots obtained for PH-700 using data acquired at 0.1 V and 0.5 V vs. RHE.

Figure 6(b) shows the dependence of ORR activity ($|i_{0.5}|$, defined as the current corresponding to a potential of 0.5 V) on CPAT temperature. The $|i_{0.5}|$ values of HH-series carbons ranged from 0.02 to 0.03 mA cm^{-2} regardless of pretreatment temperature, while the $|i_{0.5}|$ of PH-series carbons reached 1.28 mA cm^{-2} at 700 °C and then decreased, i.e., was maximal for PH-700. Figure 6(c) shows Koutecky-Levich plots obtained for PH-700, revealing that at 0.5 V vs. RHE, the number of electrons transferred during the ORR approximately equaled three and approached a value of four at 0.1 V vs. RHE.

Notably, PN-doped (PH-series) carbons exhibited higher ORR activity than N-doped (HH-series) carbons. As N-free P-doped carbon could not be prepared from FA, P-doped carbon was prepared from poly(furyl alcohol) (PFA) to examine the effects of P-only doping on ORR activity. The ORR activity of P-doped PFA-derived carbon was higher than that of non-doped PFA-derived carbon (Fig. 7).

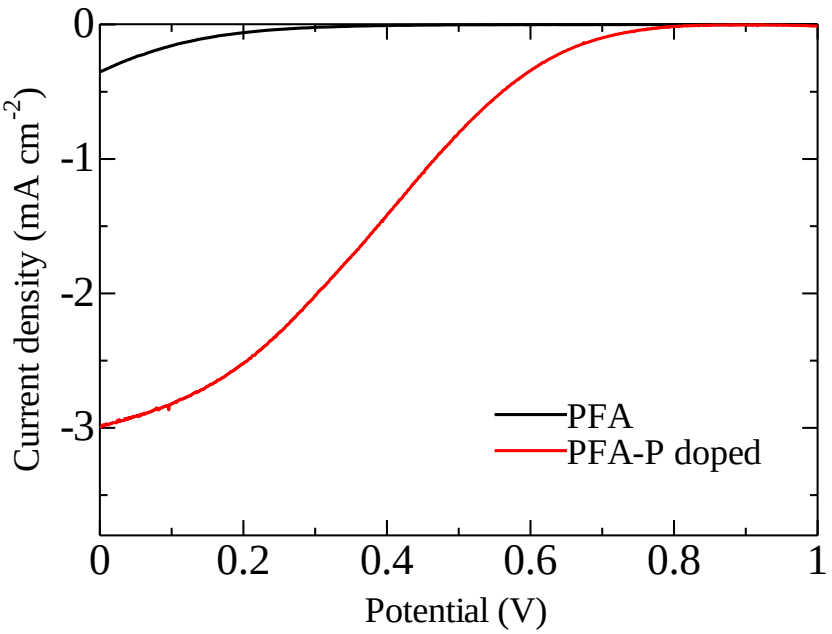

Figure 7: ORR voltammograms of various PFA-derived carbons.

Next, we correlated ORR activity with BET-SSA, XPS-determined N and P contents, and the work function. Notably, ORR activity was not correlated with BET-SSA but was correlated with the relative contents of P2 (Fig. 8(a)) and P3 (Fig. 8(b)) species, with an even better correlation obtained between ORR activity and the sum of P2 and P3 contents (Fig. 8(c)). Finally, the work function was strongly correlated with ORR activity, as shown in Fig. 5(b).

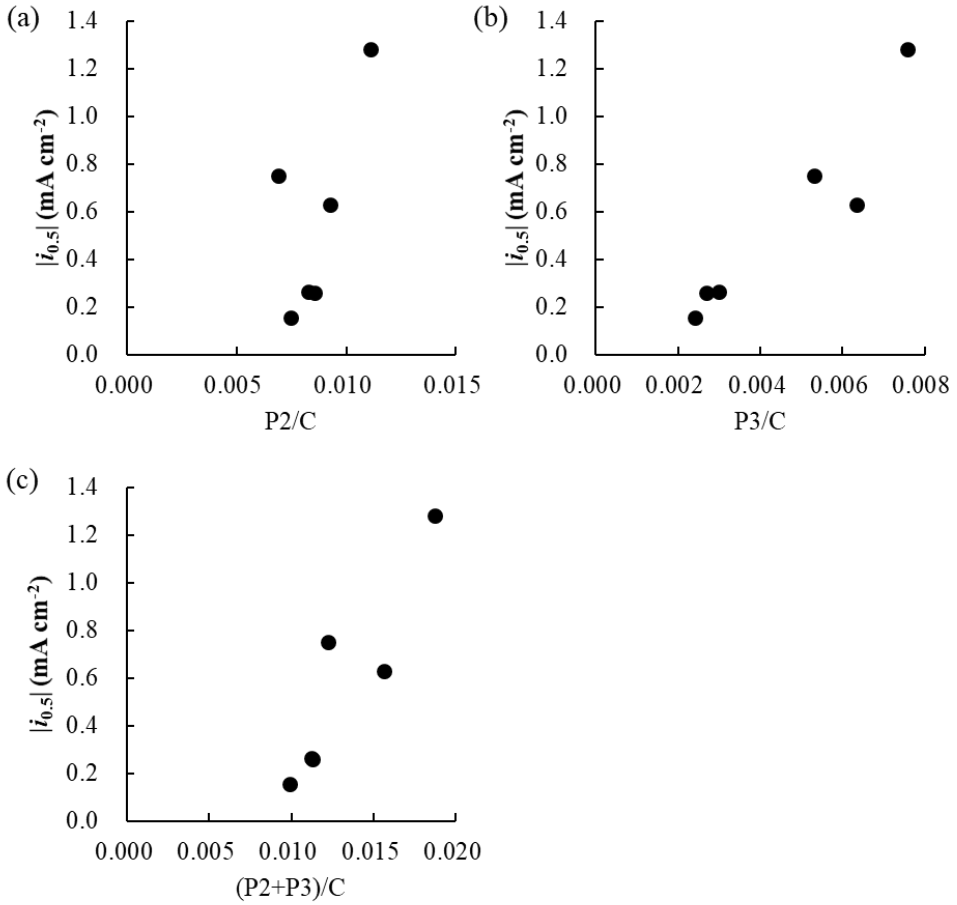

Figure 8: Correlation of ORR activity (represented by $i_{0.5}$) with (a) P2/C, (b) P3/C, and (c) (P2+P3)/C molar ratios.

Discussion

Doping of P into FA by CPAT

Differences between the N chemical states of P- and H-series precursors can be understood by considering the chemical interactions (possibly of the acid-base type) of PA with N atoms in FA, as evidenced by the correlation between P/C and N/C ratios (Fig. 1). The N 1s spectra of P-series precursors prepared at temperatures of ≥ 400 °C had a shape different from that of the corresponding

H-series precursor spectra, and 400 °C was thus taken as the onset of PA action. Interestingly, the nature of this action depended on CPAT temperature, i.e., N loss was promoted at 400 °C, precursor co-doping with N and P atoms was promoted at 400–700 °C, and the increase of BET-SSA accompanied by the decrease of N and P content was promoted above 800 °C. As a result, maximum N and P contents were obtained at a CPAT temperature of 700 °C. This behavior agreed with the results of a previous study, where the increase of BET-SSA was shown to be accompanied by the sublimation of elemental P above 800 °C.[32] As the initial aim of CPAT was to introduce P into carbons rather than to increase their BET-SSAs, the temperature of 700 °C was viewed as optimal. Finally, it was concluded that PN-doped carbon precursors can be obtained by applying CPAT to other N-containing organic compounds if a proper CPAT temperature is selected.

Chemical aspects of PN-doped carbons

The disappearance of the correlation between P/C and N/C ratios (Fig. 1) after carbonization indicated that the latter process irreversibly destroyed interactions between N and P atoms. Additionally, the P/C ratios of PH-series carbons were correlated with those of P-series precursors, whereas no such correlation was observed for N/C ratios, which highlighted the need for an in-depth investigation of the chemistry involved at different preparation stages.

PN-doped (PH-series) carbons had a lower content of pyridinic N than HH-series carbons (Fig. 4(a) and (b)), i.e., P-doping suppressed the formation of this type of N atoms. This behavior contradicted the results of previous studies on

PN-doped carbons, which reported the facile formation of pyridinic N upon P-doping. For example, Gao et al. prepared PN-doped carbon by carbonization of an ionic liquid synthesized from *N*-methylimidazole and PA and reported the selective formation of pyridinic N due to the introduction of P.[33] Li et al. reported that carbon obtained by carbonization of P-doped aniline–coated single-wall carbon nanotubes was rich in pyridinic N,[34] while Razmjooei et al. described the influence of P-doping on the formation of pyridinic and pyrrole-type N in N, S, P-doped carbon.[24]

The 400.5 eV peak observed in the N 1s spectra of PH-series carbons has traditionally been assigned to pyrrole/pyridone-type N. The electron configuration of pyridinic N can be described as follows: two out of five N valence electrons are used for σ-bond formation, two more electrons form an unshared electron pair, and the remaining electron is donated to the π-electron system. Conversely, in the case of pyrrolic N, two valence electrons are used to form C–N–C σ-bonds, one electron is used to form the N–H bond, and the remaining two electrons are donated to the π-electron system. These differences in the number of electrons supplied to the π-electron system result in differences in N 1s peak binding energies. Strelko et al. conducted quantum chemical calculations to characterize N-doped graphene, revealing that the electronic states of hydrogenated pyridinic N and the three-coordinated N located in the valley at the zigzag edge of graphene are similar to that of pyrrole-type N.[21]

Detailed analysis of N 1s and P 2p spectra showed that the presence of N–P bonds in carbonized products can be excluded and demonstrated that P was mainly present as –C–PO_2. However, it was difficult to prove the presence of P–

N and P=N bonds by analysis of N 1s spectra, as binding energy similarities between N–P moieties (398.5 eV) and pyridinic N and between N=P moieties (401.3 eV) and quaternary N made unambiguous assignments impossible.[35-36] Thus, as the N 1s spectra of PH-series carbons indicated the absence of N–P and N=P bonds, we concluded that these carbons did not contain the above moieties. Regarding P 2p spectra, the main species were identified as P2 (132.5 eV; –C–PO_2) and P3 (133.2 eV; –C–PO_3). As the P–N signal usually appears at 133.5 eV and overlaps with that of P3, PH-series carbons were concluded to contain P2 and P3 as major species and feature no N–P moieties.

Factors determining ORR activity

As electrocatalytic ORR is a heterogeneous reaction occurring on solid surfaces, the overall catalytic activity is governed by the surface area involved in the reaction and the type and surface density of active sites. Herein, the ORR activity of PH-series carbons was found to be only weakly influenced by BET-SSA but was rather determined by the abundances of P2 and P3 species, i.e., by the contents of P atoms directly bonded to one or two carbon atoms. Previously, the enhanced ORR activity of PN-doped carbons was ascribed to an increase of asymmetric spin density,[24-25, 37] electron transfer from N or P to C,[33] changes of oxygen adsorption ability,[34, 38] and the formation of pyridinic N active sites due to P-doping.[34] In our case, the last reason, namely the formation of pyridinic N, can be ruled out, while further studies are required to confirm/disprove the influence of oxygen adsorption properties. At this point, it

is worth noting that our previous investigations of the relationship between the ORR activity and oxygen adsorption properties of warped graphitic layers (obtained by oxidative heat treatment of fullerene extraction residues) demonstrated that these two parameters are well correlated.[39]

ORR activity was well correlated with the work function (Fig. 5(b)), which represents the energy of the Fermi level with respect to that of the vacuum level. Several reports on the relationship between the work function of cathode catalysts and their ORR activity demonstrated that the former parameter strongly influences the latter and affects electron transfer in elementary reaction steps. As the Fermi level is the highest-energy electronic level of a given solid, the ORR reaction proceeds spontaneously when this level exceeds the ORR standard potential of 5.6 eV.[40-42] As shown in Fig. 5(a), PH-series carbons had work functions of less than 5.6 eV and could therefore spontaneously promote the ORR.

Conclusion

Herein, we applied controlled phosphoric acid treatment (CPAT) of folic acid (FA) to prepare P-doped precursors, which were then carbonized to afford PN-doped carbons as oxygen reduction reactions (ORR) catalysts. Essentially, FA was heated in the presence of phosphoric acid at an optimal temperature of 700 °C to maximize the P content of precursors before the occurrence of chemical activation. The P/C ratio of precursors was found to be positively correlated with that of the corresponding carbons and carbon ORR activity. In contrast to

previous studies, where ORR activity has been largely attributed to the presence of pyridinic N–based active sites, the enhanced ORR activity of our carbons was ascribed to the presence of –C–PO_2 and C–PO_3 moieties. Moreover, this activity increased with decreasing work function of carbons. Given that an optimal treatment temperature is selected, we believe that the CPAT technique can be applied to all types of N-containing compounds, e.g., naturally occurring ones. However, fundamental studies on the kinetics and mechanisms of ORR activity enhancement induced by PN-doping are required to clarify the remaining questions and will be conducted in due course.

Experimental

CPAT

N- and P-containing precursors were prepared by heating FA in the presence of PA. Typically, FA (1 g; Wako, Wako Special Grade) was ground with ethanolic PA (85 wt%, 1 g; Wako, Wako Special Grade) using a mortar and pestle, and the obtained mixture was placed in a furnace, heated to 400–800 °C in a flow of N_2 at a rate of 50 °C min^{-1}, and then held at this temperature for 1 h. The carbonized samples were then pulverized at 650 rpm for 50 min using a planetary ball mill (P-7, Fritsch), sieved to retrieve particles smaller than 106 μm in diameter, vigorously stirred in deionized water at 80 °C for 1 h, and dried to obtain P-T specimens (T = CPAT temperature). Controls were prepared in the same manner without the addition of PA and were referred to as H-T (T = pretreatment temperature).

Carbonization

The doped and control precursors were carbonized at 1000 °C for 1 h in a stream of N_2 to afford PH-T and HH-T specimens, respectively (T = treatment temperature). Moreover, carbons were also prepared by directly heating FA or PA-FA mixtures to 1000 °C (H-1000 and P-1000 samples, respectively). To study the influence of P-only doping, the above carbonization procedure was applied to poly(furfuryl alcohol) (PFA). Two types of PFA-based carbons were prepared by using hydrochloric or phosphoric acids as polymerization initiators (non-doped and P-doped PFA carbons, respectively).

Electrochemical methods

The ORR activity of carbons was probed by rotating disk electrode voltammetry. The working electrode was prepared by loading the catalyst (200 μg cm^{-2}) on a glassy carbon disk electrode, while the reversible hydrogen electrode (RHE) and a glassy carbon plate were employed as reference and counter electrodes, respectively. The electrolyte corresponded to a 0.5 M solution of H_2SO_4 in de-ionized water. Net ORR voltammograms were obtained as the difference between linear sweep voltammograms recorded at 1500 rpm in O_2-saturated and N_2-saturated electrolytes. Koutecky-Levich analysis was conducted for a selected sample by taking D_{O2} = 1.40 × 10^{-5} cm^2 s^{-1} and v = 1.00 × 10^{-2} cm^2 s^{-1}.[43] Oxygen concentration was determined using an optical oxygen meter (FireStingO_2, Pyro Science GmbH) as C_{O2} = 1.20 × 10^{-6} mol cm^{-3}.

The membrane-electrode assembly was fabricated as follows. The catalyst ink, i.e., the dispersion of the catalyst in Nafion solution ((5 wt% solution of lower aliphatic alcohols, Aldrich), ionomer:catalyst weight ratio ~0.7:1) was sprayed onto a diffusion layer (29BC, SGL CARBON GmbH). A Pt/C catalyst was used as the anode (catalyst loading = 0.3 mg cm^{-2}), and PH-700 was used as the cathode (catalyst loading = 3.5 mg cm^{-2}). A 5-cm^2 cell was used for fuel cell testing. Polarization curves were obtained at a cell temperature of 80 °C, a back pressure of 200 kPa, and a reactant gas relative humidity of 100% using H_2 (1 L min^{-1}) and O_2 (1 L min^{-1}) as anode and cathode gases, respectively.

Characterization techniques

Brunauer-Emmett-Teller (BET) surface area was evaluated by N_2 adsorption measurements (BELSORP Max, Microtrac BEL). Samples were placed in a tube and degassed at 200 °C for 2 h under dynamic vacuum conditions. C 1s, N 1s, O 1s, and P 2p core-level X-ray photoelectron spectra were recorded using Mg K_α radiation (Kratos AXIS-NOVA, Shimadzu Corp.). Generally, the charge-up shift correction was performed by setting the C 1s peak binding energy to 284.5 eV. Charge-up corrections for PA-400, 500, and 600 were performed by bringing these samples into contact with In foil and setting the In 3d peak binding energy to 451.4 eV. Work functions were measured under N_2 by a vibration capacity electrometer (DCU series10, KP Technology).

Acknowledgments

This study was conducted at the Nisshinbo Endowed Laboratory in Gunma University, Japan. We also thank Editage (www.editage.jp) for English language editing.

References

1. Banham, D.; Choi, J. Y.; Kishimoto, T.; Ye, S. *Adv. Mater.* **2019**, 1804846. doi: 10.1002/adma.201804846

2. Toda, T.; Igarashi, H.; Watanabe, M. *J. Electroanal. Chem.* **1999,** *460*, 258–262. doi: 10.1016/S0022-0728(98)00361-1

3. Zhang, J.; Lima, F.; Shao, M.; Sasaki, K.; Wang, J.; Hanson, J.; Adzic, R. *J. Phys. Chem. B* **2005,** *109*, 22701–22704. doi: 10.1021/jp055634c

4. Jasinski, R. *Nature* **1964,** *201*, 1212–1213. doi: 10.1038/2011212a0

5. Jahnke, H.; Schönborn, M.; Zimmermann, G. Organic Dyestuffs as Catalysts for Fuel Cells. In *Physical and Chemical Applications of Dyestuffs*; Springer: Berlin, Germany, 1976; pp 133–181.

6. Lefèvre, M.; Dodelet, J.; Bertrand, P. *J. Phys. Chem. B* **2002,** *106*, 8705–8713. doi: 10.1021/jp020267f

7. Lefèvre, M.; Proietti, E.; Jaouen, F.; Dodelet, J.-P. *Science* **2009,** *324*, 71–74. doi: 10.1126/science.1170051

8. Ozaki, J.; Imashiro, Y. *Electrochemistry* **2015,** *83*, 319–325. doi: 10.5796/electrochemistry.83.319

9. Ozaki, J.; Nozawa, K.; Yamada, K.; Uchiyama, Y.; Yoshimoto, Y.; Furuichi, A.; Yokoyama, T.; Oya, A.; Brown, L.; Cashion, J. *J. Appl. Electrochem.* **2006,** *36*, 239–247. doi: 10.1007/s10800-005-9054-2

10. Ozaki, J.; Tanifuji, S.-i.; Furuichi, A.; Yabutsuka, K. *Electrochim. Acta* **2010,** *55*, 1864–1871. doi: 10.1016/j.electacta.2009.10.037

11. Ozaki, J.; Anahara, T.; Kimura, N.; Ida, C.; Oya, A.; Bokhonov, B. B.; Korchagin, M. A.; Sakashita, M. *Tanso* **2007,** *2007*, 153–157. doi: 10.7209/tanso.2007.153

12. Banham, D.; Kishimoto, T.; Sato, T.; Kobayashi, Y.; Narizuka, K.; Ozaki, J.; Zhou, Y.; Marquez, E.; Bai, K.; Ye, S. *J. Power Sources* **2017,** *344*, 39–45. doi: 10.1016/j.jpowsour.2017.01.086

13. Banham, D.; Kishimoto, T.; Zhou, Y.; Sato, T.; Bai, K.; Ozaki, J.; Imashiro, Y.; Ye, S. *Sci. Adv.* **2018,** *4*, eaar7180. doi: 10.1126/sciadv.aar7180

14. “Ballard to Offer World’s First PEM Fuel Cell Product Using Non Precious Metal Catalys”, Sep 12, 2017, Vancouver, Canada.

http://ballard.com/about-ballard/newsroom/news-releases/2017/09/13/ballard-to-offer-world-s-first-pem-fuel-cell-product-using-non-precious-metal-catalyst (accessed 28th Mar).

15. ” Notice of development of new application for carbon alloy catalyst, a replacement for platinum catalysts”, September 22, 2017, Tokyo, Japan. https://www.nisshinbo.co.jp/english/news/pdf/1653_1_en.pdf. (accessed 28th Mar).

16. Maldonado, S.; Stevenson, K. J. *J. Phys. Chem. B* **2005,** *109*, 4707–4716. doi: 10.1021/jp044442z

17. Shui, J.; Wang, M.; Du, F.; Dai, L. *Sci. Adv.* **2015,** *1*, e1400129. doi: 10.1126/sciadv.1400129

18. Ozaki, J.; Kimura, N.; Anahara, T.; Oya, A. *Carbon* **2007,** *45*, 1847–1853. doi: 10.1016/j.carbon.2007.04.031

19. Zhang, J.; Dai, L. *Angew. Chem., Int. Ed. Engl.* **2016,** *55*, 13296–13300. doi: 10.1002/anie.201607405

20. Choi, C. H.; Chung, M. W.; Park, S. H.; Woo, S. I. *Phys. Chem. Chem. Phys.* **2013,** *15*, 1802–1805. doi: 10.1039/c2cp44147k

21. Strelko, V. V.; Kuts, V. S.; Thrower, P. A. *Carbon* **2000,** *38*, 1499–1503. doi: 10.1016/S0008-6223(00)00121-4

22. Gao, J.; Ma, N.; Tian, J.; Shen, C.; Wang, L.; Yu, P.; Chu, Y.; Liu, W.; Tan, X.; Li, X.; Yin, Z. *J. Solid State Electrochem.* **2017,** *22*, 519–525. doi: 10.1007/s10008-017-3785-y

23. Li, R.; Wei, Z. D.; Gou, X. L. *ACS Catal.* **2015,** *5*, 4133–4142. doi: 10.1021/acscatal.5b00601

24. Razmjooei, F.; Singh, K. P.; Song, M. Y.; Yu, J.-S. *Carbon* **2014,** *78*, 257–267. doi: 10.1016/j.carbon.2014.07.002

25. von Deak, D.; Biddinger, E. J.; Luthman, K. A.; Ozkan, U. S. *Carbon* **2010,** *48*, 3637–3639. doi: 10.1016/j.carbon.2010.05.022

26. Li, J. C.; Hou, P. X.; Cheng, M.; Liu, C.; Cheng, H. M.; Shao, M. H. *Carbon* **2018,** *139*, 156–163. doi: 10.1016/j.carbon.2018.06.023

27. Puziy, A. M.; Poddubnaya, O. I.; Ziatdinov, A. M. *Appl. Surf. Sci.* **2006,** *252*, 8036–8038. doi: 10.1016/j.apsusc.2005.10.044

28. Rosas, J. M.; Bedia, J.; Rodríguez-Mirasol, J.; Cordero, T. *Fuel* **2009,** *88*, 19–26. doi: 10.1016/j.fuel.2008.08.004

29. Zuo, S.; Yang, J.; Liu, J.; Cai, X. *Fuel Process. Technol.* **2009,** *90*, 994–1001. doi: 10.1016/j.fuproc.2009.04.003

30. Fierro, V.; Torné-Fernández, V.; Montané, D.; Celzard, A. *Thermochim. Acta*

2005, *433*, 142–148. doi: 10.1016/j.tca.2005.02.026

31. Wang, X. J.; Zhou, J. W.; Fu, H.; Li, W.; Fan, X. X.; Xin, G. B.; Zheng, J.; Li, X. G. *J. Mater. Chem. A* **2014,** *2*, 14064–14070. doi: 10.1039/c4ta01506a

32. Puziy, A. M.; Poddubnaya, O. I.; Socha, R. P.; Gurgul, J.; Wisniewski, M. *Carbon* **2008,** *46*, 2113–2123. doi: 10.1016/j.carbon.2008.09.010

33. Myglovets, M.; Poddubnaya, O. I.; Sevastyanova, O.; Lindstrom, M. E.; Gawdzik, B.; Sobiesiak, M.; Tsyba, M. M.; Sapsay, V. I.; Klymchuk, D. O.; Puziy, A. M. *Carbon* **2014,** *80*, 771–783. doi: 10.1016/j.carbon.2014.09.032

34. Gao, J.; Ma, N.; Tian, J.; Shen, C.; Wang, L.; Yu, P.; Chu, Y.; Liu, W.; Tan, X.; Li, X.; Yin, Z. *J. Solid State Electrochem.* **2018,** *22*, 519–525. doi: 10.1007/s10008-017-3785-y

35. Li, J.-C.; Hou, P.-X.; Cheng, M.; Liu, C.; Cheng, H.-M.; Shao, M. *Carbon* **2018,** *139*, 156–163. doi: 10.1016/j.carbon.2018.06.023

36. Perry, W. B.; Schaaf, T. F.; Jolly, W. L. *J. Am. Chem. Soc.* **1975,** *97*, 4899–4905. doi: 10.1021/ja00850a019

37. Hulicova-Jurcakova, D.; Seredych, M.; Lu, G. Q.; Kodiweera, N. K. A. C.; Stallworth, P. E.; Greenbaum, S.; Bandosz, T. J. *Carbon* **2009,** *47*, 1576–1584. doi: 10.1016/j.carbon.2009.02.006

38. Choi, C. H.; Park, S. H.; Woo, S. I. *ACS Nano* **2012,** *6*, 7084–7091. doi: 10.1021/nn3021234

39. Yu, D. S.; Xue, Y. H.; Dai, L. M. *J. Phys. Chem. Lett.* **2012,** *3*, 2863–2870. doi: 10.1021/jz3011833

40. Takigami, M. K., R.; Ishii, T.; Imashiro, Y.; Ozaki, J. submitted to *Beilstein J. Nanotechnol*.

41. Liu, M.; Liu, J.; Li, Z.; Wang, F. *ACS Appl. Mater. Interfaces* **2018,** *10*, 7052–7060. doi: 10.1021/acsami.7b16549

42. D. Landolt, *Corrosion and surface chemistry of metals*; EPFL Press: Lausanne, Switzerland, 2007; vol. 45, pp 57–58.

43. Winget, P.; Cramer, C. J.; Truhlar, D. G. *Theor. Chem. Acc.* **2004,** *112*, 217–227. doi: 10.1007/s00214-004-0577-0